Multiple spintronic functionalities into single zinc-ferrous ferrite thin films

Murtaza Bohra, Rémi Arras, Jean-Francois Bobo, Vidyadhar Singh, Naresh Kumar, Hsiung Chou

Multiple spintronic functionalities into single zinc-ferrous ferrite thin films

Murtaza Bohra[a], Rémi Arras[b], Jean-Francois Bobo[b], Vidyadhar Singh[c], Naresh Kumar[d], Hsiung Chou[e,*]

[a] Mahindra University École Centrale School of Engineering (MEC), Survey Number 62/1A, Bahadurpally Jeedimetla, Hyderabad 500043, Telangana, India
[b] CEMES, Université de Toulouse, CNRS, UPS, 29 rue Jeanne-Marvig, F-31055 Toulouse, France
[c] Department of Physics, Jai Prakash University, Chapra 841301, Bihar, India
[d] Motilal Nehru National Institute of Technology Allahabad, Prayagraj 211004, India
[e] Department of Physics, and Center of Crystal Research, National Sun Yat-sen University, Kaohsiung 80424, Taiwan

A B S T R A C T

The ability to combine multiple spintronic properties in the $Zn_xFe_{3-x}O_4$ system with different variants of its chemical composition offers a new and tantalizing route towards homodevices. This is mainly due to the advantage of varying the Zn component of $Zn_xFe_{3-x}O_4$, which leads to the possibility of preserving spinel symmetry (within 5% lattice mismatch) while changing the material properties from a ferrimagnetic half-metal (x = 0) to an insulating paramagnet (x = 1). Here we demonstrate that $Zn_xFe_{3-x}O_4$ thin films, grown from a $ZnFe_2O_4$ single phase target, laser-ablated under a reduced atmosphere, exhibits a reduction of Zn content, a large $4\pi M_S$ (6.5 kG), very low resistivity (25 mΩ cm) and a Verwey transition, all of which can be engineered by an appropriate choice of growth temperature. All these spectacular properties are confirmed by *ab initio* calculations and can be attributed to the inverse structure of $[Zn_x^{+2}Fe_{1-x}^{+3}]_A[Fe_{1+y}^{+3}Fe_{1-y}^{+2}]_BO_{4-\delta}$, where the reduced Fe^{+2} ions along with Fe^{+3} occupy the octahedral sites while the Zn^{+2} and inverted Fe^{+3} sit in the tetrahedral sites. Phase formation in laser ablated $Zn_xFe_{3-x}O_4$ thin films are different compared to the bulk thermal equilibrium, and shows that there is a competition between the reduction of Zn and the formation of O vacancies at various growth temperature zones.

1. Introduction

Standard electronic devices have the benefit of using Si for nearly all of their components. Except for a few exceptions, such as the insulating layers and metal electrodes, the n-, p- and intrinsic-type semiconducting layers can all be formed simply by varying the doping in Si and by preserving similar lattice constants, regardless of the degree of doping; these layers can be stacked to form homo-structures. These advantages could be adapted to spintronics applications by using the Zn doped Fe_3O_4 ($Zn_xFe_{3-x}O_4$) as the building block of homodevices. Fe ions are in 2 + and 3 + mixed-valence states for x = 0 (Fe_3O_4) and x < 1 ($Zn_xFe_{3-x}O_4$) and are called as Ferrous-ferrite and Zn-ferrous-ferrite, respectively. Only when x = 1 ($ZnFe_2O_4$), all Fe ions are in 3 + state and this compound is called as Zn-ferrite. With these variant doping, we can access the beneficial properties of the $Zn_xFe_{3-x}O_4$ families which are needed for spintronics: lattice constants which slightly vary as a function of the doping, as well as the existence of various magnetic properties and tunable electric conductivities [1,2]. One of the end members of this family, the Fe_3O_4 (x = 0), is a half-metal with an inverse spinel structure and a Curie temperature ($T_C \geq 850$ K) much higher than the usual operating temperature, which makes this oxide one of the best candidates for oxide spintronics [3]. The other end-member $ZnFe_2O_4$ (x = 1), on the contrary, is a paramagnetic insulator [4]. The lattice constants of Fe_3O_4 and $ZnFe_2O_4$ are 8.39 Å and 8.44 Å, respectively, creating a lattice mismatch of only 5% [5]. As we will demonstrate later, intermediate compositions can even allow an increase in the saturation magnetization as compared to the ideal Fe_3O_4 compound. Yet, studies of thin-layer $Zn_xFe_{3-x}O_4$ have not been so intensive, and much remains to be learnt concerning their potential for monolithic spintronic architectures.

When the Zn-ferrites ($ZnFe_2O_4$) were grown into a nanostructured thin film, its spinel symmetry and insulating properties were maintained to the same as the bulk but its magnetic property was changed to ferrimagnetic [6]. This property has been attributed

* Corresponding author.
E-mail address: hchou@mail.nsysu.edu.tw (H. Chou).

to a certain amount of cation inversion (some Fe^{+3} ions of octahedral B-sites (*Oh*) migrate to tetrahedral A-sites (*Td*) and *vice versa* for Zn^{+2}). However, the preparation of mixed-valence $Zn_xFe_{3-x}O_4$ ($x < 1$) thin films with desired properties remains troublesome owing to the difficult control of a specific Fe^{+2}/Fe^{+3} ratio, the normal or inverse structure, and the disorder distributions of Zn^{2+} and Fe^{2+} and Fe^{3+} within one *Td* and two *Oh* sites [7–10]. Park et al. [11] grew $Zn_xFe_{3-x}O_4$ film films on Al_2O_3 substrates from the targets of various composition of x = 0.0, 0.2, 0.4 and 0.5. Based on the fact that the crystal lattice of cubic $Zn_xFe_{3-x}O_4$ film extended as the increasing of x and they followed the model [12,13] that the doped Zn^{2+} replaces the Fe^{3+} ion at the tetrahedral sites forming an inverse $(Zn,Fe)Fe_2O_4$ spinel. Nevertheless, in order to remain electrically neutral, a certain amount of oxygen vacancies must coexist. Very few reports on $Zn_xFe_{3-x}O_4$ thin films have been published regarding control over oxygen and zinc non-stoichiometry, but it is not clear whether such films genuinely formed the $Zn_xFe_{3-x}O_4$ phase [8–10] with their composition the same as the nominal composition of the targets or if they merely ended up in the Fe_3O_4 phase. Therefore, in this paper, we undertake a detailed study of the growth conditions of $Zn_xFe_{3-x}O_4$ and Fe_3O_4 thin films. We also deployed the well-known 'Verwey transition of Fe_3O_4' [7,14] as an indicator of phase purity check in these films through a magnetic study.

2. Experimental methods

$Zn_xFe_{3-x}O_4$ and Fe_3O_4 thin films (~500 nm thick) were pulse laser ablated (PLA) from $ZnFe_2O_4$ and α − Fe_2O_3 bulk targets, respectively. The third harmonic (355 nm) of the Nd:YAG laser, with an energy density of 2.5 J/cm^2, 10 Hz repetition rate and 5–6 ns pulse width was used. These films were grown at different substrate temperatures, T_G = room temperature (RT) to 850 °C, on fused quartz substrates under a high vacuum of 10^{-5} mbar ($P(O_2) = 2.1 \times 10^{-6}$ mbar). The crystalline structure and phase purity of each sample was judged by X-ray diffraction (XRD) and X-ray photoelectron spectroscopy (XPS) measurements. High resolution XPS spectra of oxygen, carbon, and iron were recorded after Ar+ ion etching of the sample surface for 10 min. Magnetic properties (*M-H* and *M-T* curves) were measured with in-plane film configuration by using a vibrating sample magnetometer (VSM) attached to the physical property measurement system (PPMS), after correcting for the diamagnetic contribution of the quartz substrate. Electrical resistivity was measured by a four-probe method attached with cryostat.

First-principles calculations based on the density functional theory (DFT) were performed using the Vienna *ab initio* simulation package (VASP) [15,16] with the projector augmented wave (PAW) method [17]. We used the generalized-gradient approximation to calculate the exchange-correlation energy with the version proposed by Perdew, Burke and Ernzerhof, and revised for solids (PBESol) [18]. A *U*-dependent correction [19] was added on the 3d orbitals of the Fe atoms with *U* and *J* parameters being respectively equal to 4.5 eV and 0.56 eV. The cut-off energy was set to 650 eV. Each bulk compound was modelled by using a conventional cubic spinel cell of 56 atoms, which corresponds to 8 formula units (f.u.). For each $Zn_xFe_{3-x}O_4$ structure, different cation distributions and/or magnetic orderings were tested, but we only considered cases where Zn atoms substituted for Fe atoms located in tetrahedral atomic sites. The first Brillouin zone was sampled by a 12·12·12 Monkhorst-Pack grid [20].

3. Results

XRD patterns of PLA $Zn_xFe_{3-x}O_4$ and Fe_3O_4 thin films grown at different T_G are given in Fig. 1(a). All XRD peaks were peak fitted to find their positions and use the least square fitting process to calculate their lattice constants and accuracies, as shown in Table 1. This method provided better results than the Rietveld refinement by

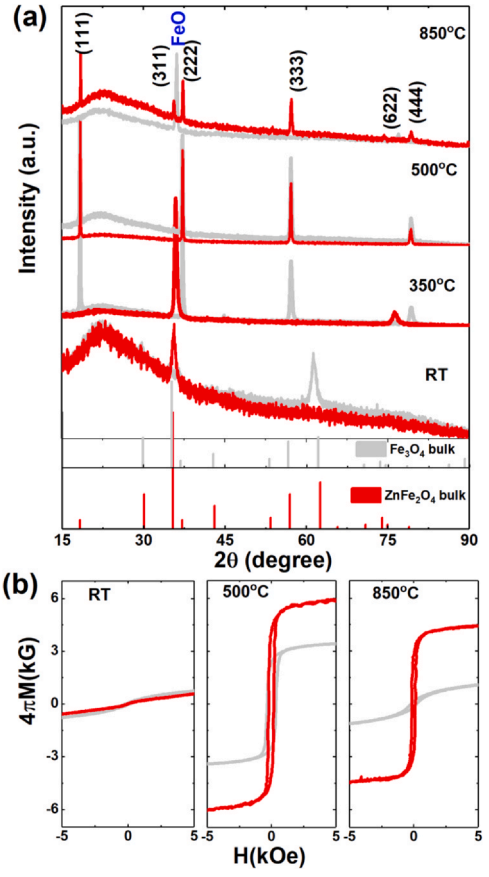

Fig. 1. (a) XRD patterns and (b) M-H loops of $Zn_xFe_{3-x}O_{4-\delta}$ and Fe_3O_4 thin films at different T_G. The bulk XRD data of $ZnFe_2O_4$ and Fe_3O_4 are also given on bottom panel of (a) for comparison.

using few textured peaks. Starting with ablation at high vacuum (HV) from an α − Fe_2O_3 target, which has 60% oxygen content, a polycrystalline Fe_3O_4 film was obtained when grown at RT. However, the observed peak intensities are quite weak in comparison to the background signal and the relative intensities of peaks do not match well with the bulk patterns such as the FeO, α − Fe_2O_3 and Fe_3O_4. This implies that the crystal structure of film grown at RT is far from perfection. Numerous defects, structure distortion and inhomogeneity in composition might exist in the RT growth film. When T_G was raised to 350 °C and 500 °C, the high-temperature thermal energy promotes the structure reconstruction process, giving rise to textured Fe_3O_4 films consisting of 57% oxygen with lattice constants of 8.372(8) and 8.371(3) for 350 °C and 500 °C grown processes, respectively. These lattice constants are smaller than the JCPD database. HV growth promoted the loss of oxygen that reduced the composition of the target, α − Fe_2O_3, to the film, Fe_3O_4. By further raising T_G to 850 °C, the film O composition was severely reduced and changed the film to the FeO phase which contains only 50% oxygen. Similarly, its lattice constant, 4.2874(2), is smaller than that of the database of FeO, 4.326(2) JCPD 89–2468. The smaller lattice constants than that of bulk value shown in JCPD database seems to be the basic property of all films in this study.

For the $Zn_xFe_{3-x}O_{4-\delta}$ film growth in HV at RT and 350 °C, only one and two peaks are observed, respectively. It is impossible to assign RT pattern to any structures while the 350 °C pattern has many possible indexing to assigned, as shown in the Table 1, indicating an expanded lattice constant due to incomplete structure with oxygen and possible Zn deficiency and mixed occupancy of Zn^{2+}, Fe^{2+} and Fe^{3+} in the *Td* and *Oh* sites. When T_G was raised to 500 °C, a good structure matching with the Fe_3O_4 appeared. Those four peaks in

Table 1
The parameters of $(ZnFe)Fe_2O_4$ and Fe_3O_4 films.

	$(ZnFe)Fe_2O_4$ Films		Fe_3O_4 Films	
Growth temp (°C)	2θ (degree)	*a* (Å)	2θ (degree)	*a* (Å)
850	Zn doped Fe_3O_4 phase (111) = 18.458(1) (311) = 35.626(4) (222) = 37.270(2) (333) = 57.204(2) (622) = 74.34(2) (444) = 79.26(1)	8.44(5)	FeO Phase (111)=36.331(6) (220) = 61.14(2) (222) = 77.04(1)	4.2874(2)
500	Zn doped Fe_3O_4 phase (111) = 18.4142(5) (222) = 37.222(1) (333) = 57.146(1) (444) = 79.192(2)	8.3847(4)	Fe_3O_4 Phase (111) = 18.368(1) (222) = 37.205(1) (333) = 57.14(3) (444) = 79.26(1)	8.371(3)
350	Zn doped FeO or $Fe_{21}O_{32}$ or Fe_3O_4 cubic phase 35.952(6) 76.310(6)	FeO Phase (111),(222) 4.3152 $Fe_{21}O_{32}$ Phase (311), (542) 8.4495 Fe_3O_4 Phase (222), (444) 8.631	Fe_3O_4 Phase (111) = 18.393(1) (222) = 37.225(4) (333) = 57.201(2) (444) = 79.26(2)	8.372 (8)
Ideal lattice constants of				
FeO	cubic	*a*=4.326(2)	JCPD 89-2468	
Fe_2O_3	Rhom.	*a*=5.04 *b*=13.75 *c*=2.7282	JCPD 89-2810	
$Fe_{21}O_{32}$	cubic	*a*=8.3457	JCPD 89-5892	
Fe_3O_4	cubic	*a*=8.3952(2)	JCPD 89-4319	

XRD can be indexed to the (n,n,n), with n being an integer, by comparing with the bulk standard databases shown in the lower two panels of Fig. 1(a) indicating a [111] textured $Zn_xFe_{3-x}O_{4-\delta}$ film. By raising T_G to 850 °C, more peaks appear, which suggests the poly-crystalline phase of $Zn_xFe_{3-x}O_{4-\delta}$ film. The XRD peaks of Fe_3O_4 and $Zn_xFe_{3-x}O_4$ films grown at 500 °C are nearly equally separated and matches very well with their bulk standards, that both films are cubic in structure. Whether Zn successfully doped in Fe_3O_4 or not, the simplest way is comparing the lattice constant of $Zn_xFe_{3-x}O_4$ to that of Fe_3O_4 grown at the same condition. As many reports have discovered that doping of Zn in Fe_3O_4 will cause an expansion of lattice constants and the ratio of doping shows a linear dependency in bulk form [21,22]. The pure Fe_3O_4 film shows a lattice constant of 8.371(3)Å that is slightly smaller than the bulk value of 8.39 Å probably due to the vacuum growth process where a certain oxygen deficiency may exist. At the same growth temperature, the lattice constant of the $Zn_xFe_{3-x}O_4$ films is 8.3847(4) Å which is ~0.014 Å larger than the Fe_3O_4 film. This difference is larger than the errors of both lattice constants. This larger lattice constant best proves the doping effect of $Zn_xFe_{3-x}O_4$. In the bulk form, $ZnFe_2O_4$ shows a lattice constant 0.05 Å larger than that of Fe_3O_4. The extension of the lattice constant of 0.014 Å in film form by Zn doping indicates the doping level of Zn is low. If the lattice constant of $Zn_xFe_{3-x}O_4$ is linearly proportional to doping of Zn, as shown of the results of Cheng's calculation [22] for $x = 0.00–0.75$, then the present film should have a composition of x around 0.27. The composition of the present film is not the same as the nominal composition of the target. A severe loss of Zn must be due to the high vapor pressure of Zn. This low content of Zn in $Zn_xFe_{3-x}O_4$ film is close to the detection limit of EDS. Instead of EDS, we use lattice constants, magnetization and XPS measurements to estimate the most likely concentration of Zn. The ionic radii of Zn^{2+} dopant, if the dopant Zn is in 2 + state, are 0.6(0.74) Å at tetrahedral(octahedral) sites and can substitute both smaller Fe^{2+} or Fe^{3+} ions either at tetrahedral or octahedral sites. XRD alone is unable to determine where is the doping site and whether an inversion of normal spinel structure.

The *M–H* loops taken at 300 K and under an in-plane external magnetic field of ± 8 kOe for $Zn_xFe_{3-x}O_{4-\delta}$ and Fe_3O_4 thin films at different T_G are plotted in Fig. 1(b). The $Zn_xFe_{3-x}O_{4-\delta}$ thin films show well defined *M–H* loops when grown at $T_G \geq 500$ °C, while more linear responses without loops can be seen for RT samples. The room temperature saturation magnetization ($4\pi M_S$) values of Fe_3O_4 and $Zn_xFe_{3-x}O_{4-\delta}$ thin films show peak-like trends to T_G, as shown in Fig. 2(a). The RT-grown polycrystalline Fe_3O_4 films have nearly zero $4\pi M_S$, plotted with circles, due to insufficient thermal energy to form a correct spinel crystal structure. For the Fe_3O_4 films grown within the best temperature window, 350 ~ 500 °C, the $4\pi M_S$ values are very close to one of the inverse spinels Fe_3O_4, as shown with the black dashed line in Fig. 2(a). With increasing T_G to 850 °C, the severe

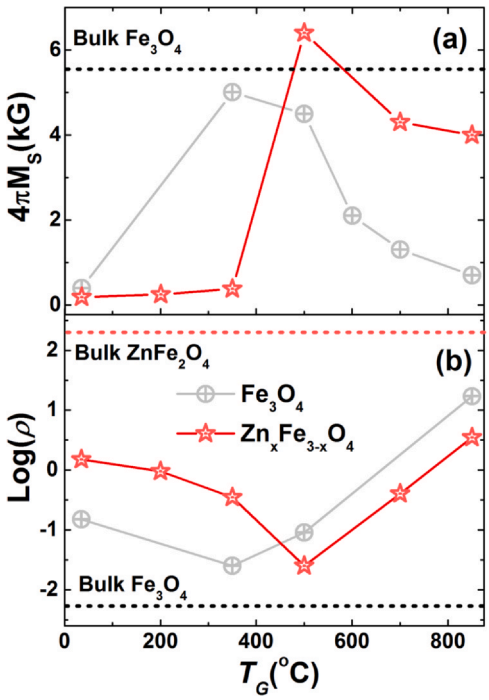

Fig. 2. (a) $4\pi M_S$ vs. T_G of $Zn_xFe_{3-x}O_{4-\delta}$ and Fe_3O_4 thin films (b) resistivity (ρ) vs. T_G data of corresponding thin films.

reduction process decomposes the film to FeO, lowering magnetization. The low temperature (between RT and 350 °C) grown $Zn_xFe_{3-x}O_{4-\delta}$ films has an imperfection in crystal structure that generates very limited perturbation to the magnetic coupling and gives rise to a small magnetization, as the red stars show in Fig. 2(a). At T_G = 500 °C, the $Zn_xFe_{3-x}O_{4-\delta}$ films show a good crystal structure and exhibit a very large $4\pi M_S$ of 6.4 kG at 300 K. The $4\pi M_S$ is slightly enhanced to 6.5 kG at 5 K, implying that Neel's temperature of the film is well above room temperature, with details provided in the supplementary material. The highest $4\pi M_S$ of bulk $Zn_xFe_{3-x}O_4$ occurs at $x = 0.2$ [21], with a value (~6.7 kG) slightly larger than the film grown at 500 °C. Therefore, the present film could have Zn content around $x = 0.2$ which matches well to our estimation based on it enlarged lattice constant. This indicates that the vacuum deposition strongly reduces both Zn and oxygen content. Moreover, PLA is a non-thermal equilibrium process, therefore, some Fe^{3+} ions may be changed to Fe^{2+} ions and, along with the Zn^{2+} ions, may be situated in *Td* or *Oh* sites. Due to HV-growth processing, oxygen vacancies may also be generated to maintain the neutrality of the $Zn_xFe_{3-x}O_{4-\delta}$ film. If all moments are strongly coupled to one another, then, according to the Goodenough-Kanamori-Anderson (GKA) rules [23–26], an AFM coupling develops between Fe ions at *Td* and *Oh* sites and an FM or AFM coupling occurs between two adjacent Fe ions at *Oh sites* (these ions being in a 3 + or a mixed (2 +, 3 +) valence state). Then the $4\pi M_S$ of the $Zn_xFe_{3-x}O_{4-\delta}$ film, if it is in a normal structure in which $Fe^{2+}$and Fe^{3+} ions occupy *Td* and *Oh* sites, respectively, and the two *Oh* sites are AFM coupling, will never be larger than the net moment of inverse Fe_3O_4. The fact that the present measurement manifests a larger $4\pi M_S$ than that of bulk Fe_3O_4 implies that the doped Zn ion must mainly replace Fe^{3+} ions at tetrahedral sites that suggest the present $Zn_xFe_{3-x}O_{4-\delta}$ films grown at 500 °C have an inverse or mixture spinel structure. With higher T_G > 500 °C, the $4\pi M_S$ decreases and, surprisingly, attains a value even smaller than that of the bulk Fe_3O_4 for the 850 °C film, which will be discussed later.

Although bulk $ZnFe_2O_4$ is an insulator, the present $Zn_xFe_{3-x}O_{4-\delta}$ films grown in HV become conductive, as shown as the red stars in Fig. 2(b). The resistivity shows a minimum value for the film grown at 500 °C with the lowest value $\rho = 2 \times 10^{-3}$ Ω-cm, which is five orders smaller than that of the bulk $ZnFe_2O_4$ (2.2×10^2 Ω cm). Importantly, the resistivity of the present $Zn_xFe_{3-x}O_{4-\delta}$ films has a trend and scale similar to Fe_3O_4 films as shown by the circles and line in Fig. 2(b). The conductive mechanism of the inverse Fe_3O_4 originates from the mixed-valence of Fe^{3+} and Fe^{2+} of the adjacent *Oh* sites, which triggered an effect analogous to the double exchange coupling [27,28]. Therefore, we expect the same effect, the mixed-valence, occurs in the present $Zn_xFe_{3-x}O_{4-\delta}$ films, where part of Fe ions in the *Oh* sites transfers from Fe^{3+} state to Fe^{2+} state. If this is the case, then the present $Zn_xFe_{3-x}O_{4-\delta}$ films could have a mixed spinel structure.

The existence of Fe^{2+} and the location of Zn^{2+} are one of the key issues to understand the magnetic structure of the present $Zn_xFe_{3-x}O_{4-\delta}$ films. The XPS Fe 2p core spectrum (shown in Fig. 3) of the 500 °C $Zn_xFe_{3-x}O_{4-\delta}$ film shows broad peaks very different to the spectrum of bulk $ZnFe_2O_4$, which has only Fe^{3+}, while very similar to Fe_3O_4 spectrum along with satellite peaks around 714 eV, demonstrating the mixed-valence of Fe^{3+} and Fe^{2+} for Fe_3O_4 and proving the co-existence of Fe^{+2} and Fe^{3+} ions in the present $Zn_xFe_{3-x}O_{4-\delta}$ films. Considering both the low resistivity and the co-existence of Fe^{+2} and Fe^{3+} ions strongly suggests the present film has a mixed spinel structure. In addition, the inset of Fig. 3 shows a comparison of the Zn 2p core spectrum at around 1021 eV for both the present film and the bulk $ZnFe_2O_4$. Both Zn spectra match perfectly for both positions and shapes, indicating that Zn atoms occupy *Td* sites [25]. The weak intensity of the Zn spectrum implies a loss of Zn due to its high vapour pressure and the HV environment during the PLA process. This agrees with our estimated Zn content in the previous paragraph.

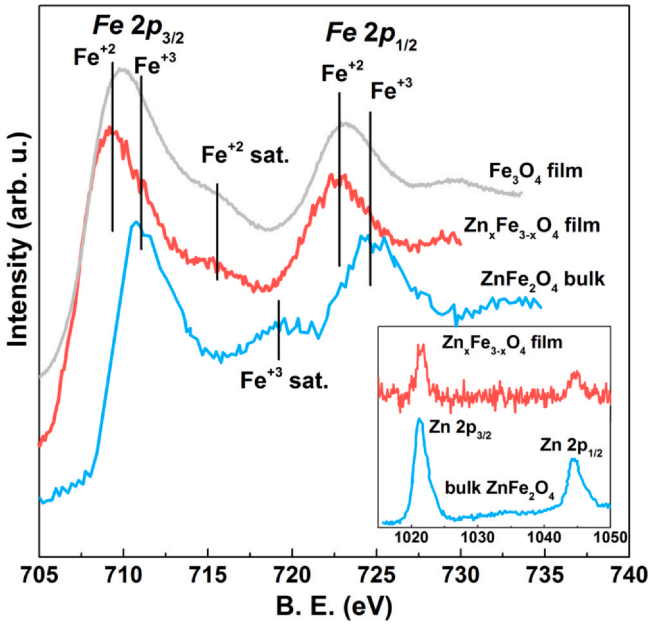

Fig. 3. Fe 2p spectra for $Zn_xFe_{3-x}O_{4-\delta}$ and Fe_3O_4 thin films at T_G = 500 °C. Inset shows Zn 2p spectra of corresponding samples. For comparison, Fe 2p and Zn 2p spectra of bulk $ZnFe_2O_4$ are also included.

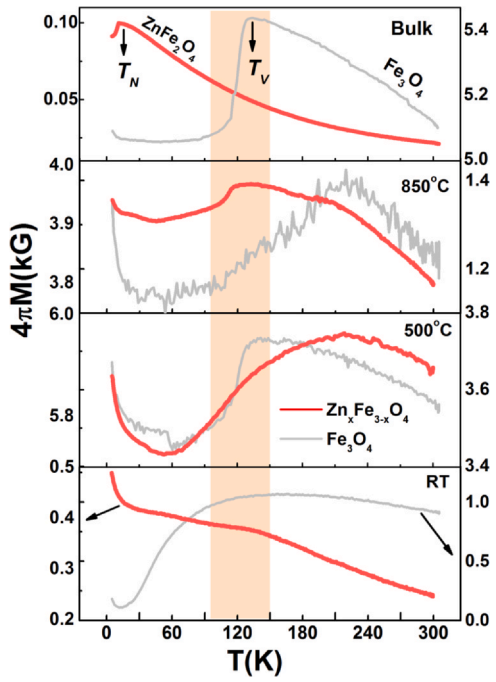

Fig. 4. M vs. T curves (at fixed field of 5 kOe) of $Zn_xFe_{3-x}O_{4-\delta}$ and Fe_3O_4 thin films at different T_G. M vs. T curves of bulk $ZnFe_2O_4$ and Fe_3O_4 on top panel are plotted for the comparison.

Since Verwey transition temperature (T_V) is extremely sensitive to the oxygen and transition metal stoichiometry of the compound [13,29,30], it is crucial to measure T_V in our $Zn_xFe_{3-x}O_{4-\delta}$ and Fe_3O_4 thin films to check the phase purity of samples. Fig. 4 shows *M-T* curves measured at fixed magnetic field of 5 kOe for films grown at different T_G. The *M-T* curves of bulk $ZnFe_2O_4$ and Fe_3O_4 are also plotted at top panel for comparison. The *M-T* curves of the Fe_3O_4 film grown at RT show a broad AFM ordering for T < 120 K, which is apparently due to the imperfect crystal structure. For 500 °C and 850 °C grown Fe_3O_4 films, a clear Verwey transition of Fe_3O_4 (~120 K)

and an AFM transition of a FeO phase (~200 K) are observed, respectively. The magnetization of RT grown $Zn_xFe_{3-x}O_{4-\delta}$ thin film increases with lowering temperature which is due to the imperfections of the crystal structure. Interestingly, when T_G is increased to 500 °C, the present $Zn_xFe_{3-x}O_{4-\delta}$ films show a broad signature of Verwey transition beginning to develop, behaviour similar to that observed by Saha et al. in $Zn_xFe_{3-x}O_4$ ($x = 0.2$) nanospheres [1]. At the highest T_G of 850 °C, a sharp Verwey transition can be seen at 120 K, akin to the single-phase Fe_3O_4 films grown at 500 °C. This gives rise to two possible results due to the severe loss of Zn and O at 850 °C growth temperature, neither of which can be distinguished by XRD in Fig. 1. The first is a transfer of the film into the Fe_3O_4 phase. The second is the formation of a solid solution of the imperfect $Zn_xFe_{3-x}O_{4-\delta}$ and the Fe_3O_4 phases. The latter is more reasonable because these films show smaller $4\pi M_S$ (Fig. 2a) and higher ρ (Fig. 2b) values compared to pure Fe_3O_4.

4. Discussions

The HV and high-temperature environments reduce the Zn content of the present films. The XPS confirms the reduction of Zn and determines that the Zn^{2+} ion must be located at *Td* site. The existence of Fe^{2+} forms a mixed-valence state of Fe^{2+} and Fe^{3+}. Because the conductivity of the sample is greatly enhanced, the mixed-valence should be located at *Oh* sites due to a double exchange coupling. From magnetic and XRD studies, the present film has an inverse structure of $[Zn_x{}^{+2}Fe_{1-x}{}^{+3}]_A[Fe_{1+y}{}^{+3}Fe_{1-y}{}^{+2}]_BO_{4-\delta}$ where the oxygen deficiency δ may or may not equal to zero if $x = y$ or $x \neq y$, respectively.

To confirm our hypothesis concerning the atomic structure and cation distribution which generated the previously-described properties, we performed DFT calculations. In Fig. 5, we report the calculated total densities of states (DOS) for better insight regarding the electronic structure. These DOS are displayed for three chemical compositions, *i.e.* of $x = 0$, 0.25 and 1; $x = 0.25$ was chosen to approximate the particular composition for which we experimentally obtained the highest magnetization.

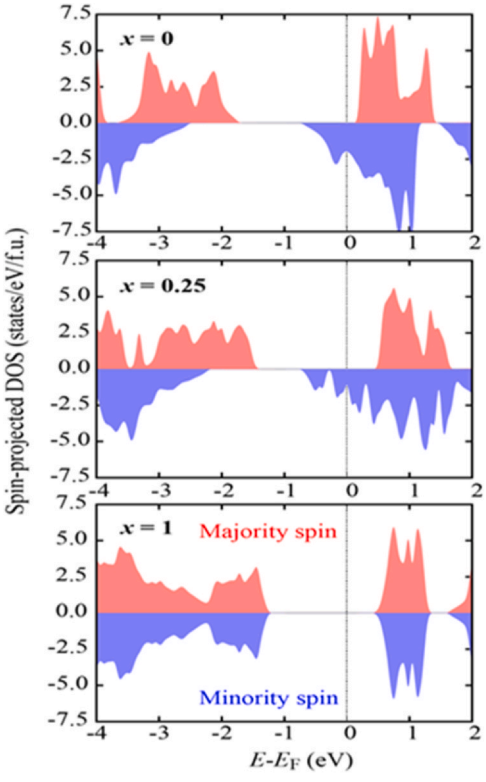

Fig. 5. Spin-projected densities of states (DOS) of the $Zn_xFe_{3-x}O_4$ bulk compound obtained from the DFT calculations and given as a function of the Zn content x.

For $x = 0$, *i.e.* pure Fe_3O_4, we considered a spinel structure with a cubic cell and we enforced all Fe atoms in *Oh* sites to remain equivalent. With these computational parameters, no charge ordering, characteristics of the insulating low-temperature phase of Fe_3O_4, are observed; the Fe cations in the *Oh* sites then possess an average oxidation degree consistent with the inverse spinel structure (of 2.5 + if we approximate it as a perfectly ionic crystal). The associated spin-projected DOS curves correspond to a half-metallic behavior, the Fermi energy E_F being located at a gap for the majority-spin electrons, while the DOS is non-null for the minority-spin electrons. The half-metallicity with a total spin magnetic moment of 4 μ_B/f.u. is in agreement with results previously reported for this compound [31,32] and comes from the inverse spinel structure with Fe^{3+} cations with a theoretical magnetic moment of − 5 μ_B in the *Td* sites, while the *Oh* sites would be equally occupied by Fe^{3+} and Fe^{2+} cations with magnetic moments respectively equal to + 5μ_B and + 4 μ_B (the spin magnetic moments calculated within the DFT are respectively −3.90 μ_B and +3.81 μ_B). For $x = 1$, we have a pure normal $ZnFe_2O_4$ phase, and the Fermi level is located within a bandgap closer to the conduction band minimum for both spin directions, making the $ZnFe_2O_4$ a perfect insulator. This is very different to Cheng's simulation [22] that the Fermi surface located right at the valence band maximum. The *Td* and *Oh* sites, respectively, are filled with Zn^{2+} and Fe^{3+} ions. The superexchange coupling between two Fe^{3+} ions at adjacent *Oh* sites induce an AFM ordering and the resulting total magnetic moment is zero when only a collinear magnetic configuration is considered. For a composition closer to pure Fe_3O_4 ($x = 0.25$), a non-zero DOS at the Fermi level suggests that the half-metallicity is preserved. The slightly lower DOS for the minority spin channel than that of Fe_3O_4 indicates that the spinel $Zn_{0.25}Fe_{2.75}O_4$ has a higher resistivity than the bulk Fe_3O_4 which matches the present experimental result, as shown in Fig. 2(b). The magnetic configuration used to fulfil the aforementioned results were $[Zn_{0.25}{}^{+2}Fe_{0.75}{}^{+3}(\downarrow)]_A[Fe_{1.25}{}^{+3}(\uparrow)Fe_{0.75}{}^{+2}(\uparrow)]_BO_4$. However, because these moments are lined up collinearly, the calculated total magnetic moment equals 5.5 μ_B/f.u. (~7.4 KG), which is higher than the measured value (~6.4 KG). This inconsistency could be in principle corrected by introducing a Yafet-Kittel canting [21] in between adjacent *Oh* sites. This canting would weaken the double exchange coupling and lower the conductivity. The canting mechanism is not certain and many possibilities such as the Dzyaloshinskii-Mariya interaction [33,34] due to a spin-orbit coupling are worthy of study. The presence of point defects such as oxygen vacancies, which would reduce more cations from Fe^{3+} to Fe^{2+} in Oh sites, or extended defects [2,35] such as antiphase boundaries [36,37], may also contribute to the measured reduction of the magnetization as compared with the theoretical value in nanocrystalline $Zn_xFe_{3-x}O_{4-\delta}$ thin films.

Based on growth conditions and various physical properties (structural, magnetic and electrical) of the $Zn_xFe_{3-x}O_{4-\delta}$ and Fe_3O_4 thin films, we can understand crystalline phase formation in three stages. Thin-film growth by laser ablation is not a thermodynamic equilibrium process but a kinetic one where the kinetic energy due to ablation and the thermal energy from the heater kinetically determine how the adatom grows on the substrate. In this study, the pressure and geometry of the system were fixed. The major parameter is the growth temperature, T_G, which can be divided into three zones, the low, medium and high-temperature zones. In the low-temperature zone, T_G = RT for Fe_3O_4 thin film and T_G = RT ~ 350 °C for $Zn_xFe_{3-x}O_{4-\delta}$ film, the thermal energy at the substrate surface is too low to form a perfect crystal. The imperfection in the crystal makes the RT Fe_3O_4 film high resistivity while imperfection reduces the resistivity of the RT $Zn_xFe_{3-x}O_{4-\delta}$ film by two orders. At the medium temperature zone, T_G = 350–500 °C for the Fe_3O_4 thin film and T_G

= 500 °C for the $Zn_xFe_{3-x}O_{4-\delta}$ film, good epitaxial films were fabricated. The resistivities of the Fe_3O_4 and $Zn_xFe_{3-x}O_{4-\delta}$ films are all reduced to ~10^{-2} Ω cm. The $4\pi M_S$ of Fe_3O_4 increases sharply to a value very close to the bulk value, while the $4\pi M_S$ reaches the maximum for the $Zn_xFe_{3-x}O_{4-\delta}$ film, which is even larger than that of the bulk Fe_3O_4. For the high-temperature zone (T_G > 500 °C), severe reductions of Zn and O form FeO and a polycrystalline $Zn_xFe_{3-x}O_{4-\delta}$ film with x nearly equal to zero. Both resistivity values climb to their highest and the $4\pi M_S$ decreases. The Verwey transition is clear for the $Zn_xFe_{3-x}O_{4-\delta}$ film as a reduction to a solid solution of $Zn_xFe_{3-x}O_{4-\delta}$ and Fe_3O_4.

5. Conclusions

Zinc-ferrous ferrites ($Zn_xFe_{3-x}O_4$) constitute a class of magnetic materials which can find many useful applications by virtue of their compatible lattice constants, high magnetization and tunable resistivity. The quality control at various stages of the thin-film growth is thus essential to take full advantage of the opportunities they can offer in terms of the design of homodevices. The film growth is a result of the competition between crystal formation and the reduction of zinc and generation of oxygen vacancies at high temperature and high vacuum. Three growth zones are identified. The low-temperature zone does not have sufficient thermal energy for the material on the surface of the substrate to form a perfect crystal. The high-temperature zone combined with a high vacuum environment promotes the reduction of Zn and generates oxygen vacancies in films. The medium temperature zone, ~500 °C, provided a perfect condition to develop optimal crystal and texture alignment. The reduction effect removes most Zn content in a reduced composition $Zn_{0.2}Fe_{2.8}O_{4-\delta}$, which shows a large $4\pi M_S$ value of 6.5 kG while it exhibits a very low resistivity value of 25 mΩ-cm, very close to the value of the bulk Fe_3O_4. This strongly implies that the film exhibits an inverted crystal structure of $[Zn_x^{+2}Fe_{1-x}^{+3}]_A[Fe_{1+y}^{+3}Fe_{1-y}^{+2}]_BO_{4-\delta}$; therefore, a Verwey-like transition is observed. The DFT calculations confirmed that the $[Zn_{0.25}^{+2}Fe_{0.75}^{+3}(\downarrow)]_A[Fe_{1.25}^{+3}(\uparrow)Fe_{0.75}^{+2}(\downarrow)]_BO_{4-\delta}$ structure gives a finite density of states at the Fermi level, resulting in conduction of the film and a larger total magnetic moment than those of the Fe_3O_4.

CRediT authorship contribution statement

Murtaza Bohra: Conceptualization, Writing – original draft, Writing – review & editing, Supervision, Project administration, Funding acquisition, **Rémi Arras:** Writing – original draft, Writing – review & editing, **Jean-Francois Bobob, Vidyadhar Singh:** Writing – original draft, **Naresh Kumard, Hsiung Chou:** Writing – original draft, Writing – review & editing.

Declaration of Competing Interest

The authors declare that they have no known competing financial interests or personal relationships that could have appeared to influence the work reported in this paper.

Acknowledgments

The authors acknowledge the International Bilateral Cooperation Division of DST, India for a grant under INT/BLG/P-14/2019 (India-Bulgaria Joint Research Projects scheme). This work was granted access to the HPC resources of CALMIP supercomputing center under the allocation 2020-p19004. The authors also acknowledge the Ministry of Science and Technology (MOST), Taiwan for financial support under Grants Nor. MOST-109-2112-M-110-012. We thank Dr. Prasad, Dr. Venkataramani and Dr. Sahu from IIT-Bombay (India) for the use of few experimental facilities. We thank Dr. Chun-Chuen Yang from National Central University, ROC, Taiwan for XRD data analysis. Dr. Bohra also expresses thanks for the NEXT/NanoX invited scientist fellowship in 2018.

References

[1] P. Saha, R. Rakshit, M. Alam, K. Mandal, Magnetic and electronic properties of Zn doped Fe_3O_4 hollow nanospheres, Phys. Rev. Appl. 11 (2019) 024059.
[2] V. Zviagin, M. Grundmann, R. Schmidt-Grund, Impact of defects on magnetic properties of spinel zinc ferrite thin films, Phys. Status Solidi B 257 (2020) 1900630.
[3] M. Bohra, N. Agarwal, V. Singh, A. Short, Review on verwey transition in nanostructured Fe_3O_4 materials, J. Nanomater. 8457383 (2019) 18.
[4] M. Srivastava, S.K. Alla, S.S. Meena, N. Gupta, R.K. Mandal, N.K. Prasad, $Zn_xFe_{3-x}O_4$ (0.01≤x≤0.8) nanoparticles for controlled magnetic hyperthermia application, N. J. Chem. 42 (2018) 7144.
[5] Q. Tian, Q. Wang, Q. Xie, L. Jiangong, Aqueous solution preparation, structure, and magnetic properties of nano-granular $Zn_xFe_{3-x}O_4$ ferrite films, Nanoscale Res. Lett. 5 (2010) 1518.
[6] M. Bohra, S. Prasad, N. Kumar, D.S. Misra, S.C. Sahoo, N. Venkataramani, Large room temperature magnetization in nanocrystalline zinc ferrite thin films, Appl. Phys. Lett. 88 (2006) 262506.
[7] Y.F. Chen, D. Spoddig, M. Ziese, Epitaxial thin film $ZnFe_2O_4$: a semi-transparent magnetic semiconductor with high curie temperature, J. Phys. D Appl. Phys. 41 (2008) 205004.
[8] D. Venkateshvaran, M. Althammer, A. Nielsen, S. Geprägs, M.S. Ramachandra Rao, S.T.B. Goennenwein, M. Opel, R. Gross, Epitaxial $Zn_xFe_{3-x}O_4$ thin films: a spintronic material with tunable electrical and magnetic properties, Phys. Rev. B 79 (2009) 134405.
[9] M. Lorenz, M. Brandt, K. Mexner, K. Brachwitz, M. Ziese, P. Esquinazi, H. Hochmuth, M. Grundmann, Ferrimagnetic $ZnFe_2O_4$ thin films on $SrTiO_3$ single crystals with highly tunable electrical conductivity, Phys. Status Solidi RRL 5 (12) (2011) 438.
[10] J. Takaobushi, H. Tanaka, T. Kawai, S. Ueda, J.-J. Kim, M. Kobata, E. Ikenaga, M. Yabashi, K. Kobayashi, Y. Nishino, D. Miwa, K. Tamasaku, T. Ishikawa, $Fe_{3-x}Zn_xO_4$ thin film as tunable high curie temperature ferromagnetic semiconductor, Appl. Phys. Lett. 89 (2006) 242507.
[11] J.W. Park, A.N. Jang, J.H. Song, C.Y. Park, Y.S. Lee, Electronic structure of Zn doped Fe_3O_4 thin films, J. Nanosci. Nanotechnol. 13 (2013) 1895.
[12] V.G. Harris, N.C. Koon, C.M. Williams, Q. Zhang, M. Abe, J.P. Kirkland, Cation distribution in NiZn-ferrite films via extended x-ray absorption fine structure, Appl. Phys. Lett. 68 (1996) 2082.
[13] P. Wang, Z. Kąkol, M. Wittenauer, J.M. Honig, Electrical properties of zinc ferrites $Fe_{3-x}Zn_xO_4$ with $0 \le x < 0.3$, Phys. Rev. B 42 (1990) 4553.
[14] M. Bohra, S. Prasad, N. Venketaramani, N. Kumar, S.C. Sahoo, R. Krishnan, Magnetic properties of magnetite thin films close to the verwey transition, J. Magn. Magn. Mater. 321 (2009) 3738.
[15] G. Kresse, J. Hafner, *Ab initio* molecular-dynamics simulation of the liquid-metal–amorphous-semiconductor transition in germanium, Phys. Rev. B 49 (1994) 14251.
[16] G. Kresse, J. Furthmüller, Efficient iterative schemes for *ab initio* total-energy calculations using a plane-wave basis set, Phys. Rev. B 54 (1996) 11169.
[17] P.E. Blöchl, Projector augmented-wave method, Phys. Rev. B 50 (1994) 17953.
[18] G.I. Csonka, J.P. Perdew, A. Ruzsinszky, P.H.T. Philipsen, S. Lebègue, J. Paier, O.A. Vydrov, J.G. Ángyán, Assessing the performance of recent density functionals for bulk solids, Phys. Rev. B 79 (2009) 155107.
[19] S.L. Dudarev, G.A. Botton, S.Y. Savrasov, C.J. Humphreys, A.P. Sutton, Electron-energy-loss spectra and the structural stability of nickel oxide: an LSDA+U study, Phys. Rev. B 57 (1998) 1505.
[20] H.J. Monkhorst, J.D. Pack, Special points for brillouin-zone integrations, Phys. Rev. B 13 (1976) 5188.
[21] C.M. Srivastava, S.N. Shringi, R.G. Srivastava, N.G. Nanadikar, Magnetic ordering and domain-wall relaxation in zinc-ferrous ferrites, Phys. Rev. B 14 (1976) 2032.
[22] Y.H. Cheng, L.Y. Li, W.H. Wang, H. Liu, S.W. Ren, X.Y. Cui, R.K. Zheng, Tunable electrical and magnetic properties of half-metallic $Zn_xFe_{3-x}O_4$ from first principles, Phys. Chem. Chem. Phys. 13 (2011) 21243.
[23] P.W. Anderson, New approach to the theory of superexchange interactions, Phys. Rev. 115 (1) (1959) 2.
[24] J.B. Goodenough, Theory of the role of covalence in the perovskite-type manganites [La, M(II)]MnO_3, Phys. Rev. 100 (2) (1955) 564.
[25] J. Kanamori, Superexchange interaction and symmetry properties of electron orbitals, J. Phys. Chem. Solids 10 (2) (1959) 87.
[26] J.B. Goodenough, Magnetism and the Chemical Bond, Interscience-Wiley, New York, 1963.

[27] C. Zener, Interaction between the d-Shells in the Transition Metals. II. Ferromagnetic compounds of manganese with Perovskite structure, Phys. Rev. 82 (3) (1951) 403.
[28] P.-G. de Gennes, Effects of double exchange in magnetic crystals, Phys. Rev. 118 (1) (1960) 141.
[29] A. Kozłowski, Z. Kąkol, Z. Tarnawski, Magnetite Fe_3O_4: the correlated electron-phonon system, Acta Phys. Pol. A 111 (2007) 537.
[30] Z. Kakol, Magnetic and transport properties of magnetite in the vicinity of the verwey transition, J. Solid State Chem. 88 (1990) 104.
[31] A. Yanase, K. Siratori, Band structure in the high temperature phase of Fe_3O_4, J. Phys. Soc. Jpn. 53 (1984) 312.
[32] Z. Zhang, S. Satpathy, Electron states, magnetism, and the verwey transition in magnetite, Phys. Rev. B 44 (1991) 13319.
[33] I. Dzyaloshinsky, A thermodynamic theory of "Weak" ferromagnetism of anti-ferromagnetics, J. Phys. Chem. Solid. 4 (1958) 241.
[34] T. Moriya, Anisotropic superexchange interaction and weak ferromagnetism, Phys. Rev. 120 (1960) 91.
[35] K.L. Salcedo Rodríguez, S.J. Stewart, P.M. Mendoza Zelis, G.A. Pasquevich, C.E. Rodríguez, Torres, role of defects on the magnetic behaviour of the geo-metrically frustrated spinel $ZnFe_2O_4$, J. Alloys Compd. 752 (2018) 289.
[36] N. Jedrecy, C. Hebert, J. Perriere, M. Nistor, E. Millon, Magnetic and magne-totransport properties of $Zn_xFe_{3-x}O_{4-y}$ thin films, J. Appl. Phys. 116 (2014) 213903.
[37] M. Bohra, V. Alman, R. Arras, Nanostructured $ZnFe_2O_4$: an exotic energy material, Nanomaterials 11 (2021) 1286.

Appendix A. Supporting information

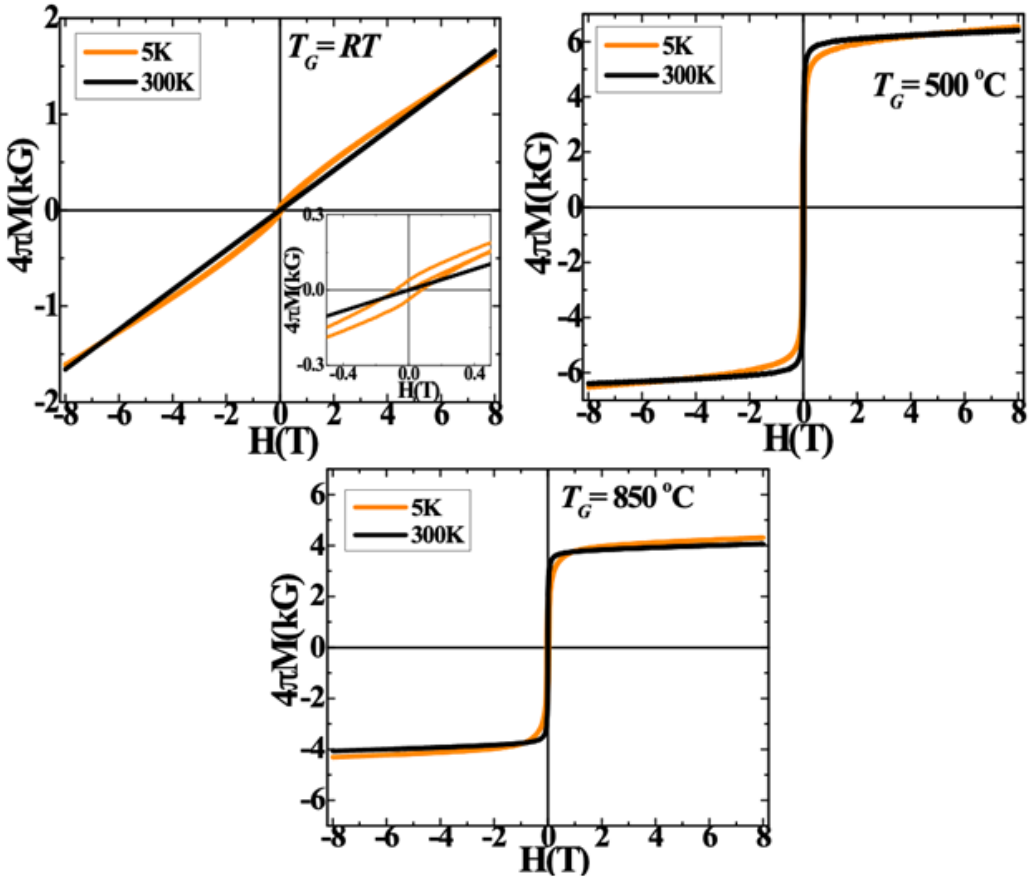

Figure S1 *M-H loops taken at 5 and 300K for $Zn_xFe_{3-x}O_4$ thin films at different growth temperature, T_G. The films grown at T_G = 350 °C shows highest $4\pi M_S$ value of 6.5 kG at 5K.*